Progress In Electromagnetics Research M, Vol. 49, 69–80, 2016

A Novel Double-Stator Permanent Magnet Generator Integrated with a Magnetic Gear

Shehu M. Salihu[1], Norhisam Misron[1, 2, *], Norman Mariun[1], Mohammad L. Othman[1], and Tsuyoshi Hanamoto[3]

Abstract—This paper presents a double-stator permanent magnet generator (DSPMG) integrated with a novel magnetic gear structure which is proposed to be used as a direct drive generator for low speed applications. Torque transmission is based on three rotors consisting of prime permanent magnet poles on the middle rotor and field permanent magnet poles on the inner and outer rotors, respectively. The proposed machine combines the function of a triple rotor magnetic gear and electrical power generator. The operating principle of the generator is discussed, and its performance characteristics are analyzed using 2-dimensional finite-element method (2D-FEM). Analysis results about its magnetic gear ratio, transmission torque, cogging torque and electrical power performance are reported. The 2-D finite element analysis results verify the proposed generator design.

1. INTRODUCTION

Research into electrical power generation from renewable energy power has attracted a lot of interest from both industries and research institutions. Typically, electrical energy is produced from a combination of prime mover and generator. Mechanical energy is used to generate an external force which rotates the generator's shaft. Examples of prime movers are automobile engines, steam turbines, gas turbines, hydro turbines, and wind turbines. A mechanical gearbox coupled to a high speed electrical machine can convert the rotational speed and torque of prime movers. However problems of size, lubrication, noise, vibration, maintenance and reliability can limit the performance of the electrical machine. For low speed operation a direct drive generator operates without a mechanical gearbox as it has high number of poles and can generate electrical power at a speed of 200 rpm. Although it eliminates the use of a gearbox it has problems of size and cost due to large number of poles including large weight and low power density. With the introduction of magnetic gears, research and development has progressed rapidly [1]. In the last 10 years, research in magnetic gears has increased because of their potential for efficient high torque transmission, inherent overload protection, lubrication-free operation and lower acoustic noise when compared with mechanical gearboxes [2]. Also various types of magnetic gears such as coaxial magnetic gears [3, 4], linear magnetic gears [5] and axial magnetic gears [6, 7] have been proposed and reported to have a transmitted torque density greater than 100 $\mathrm{kNm/m^3}$. The coaxial magnetic gear concept seems to have attracted much attention because of their good utilization of PMs and high transmission torque density. Unfortunately its complex structure makes it mechanically difficult to fabricate. Some studies on various types of magnetic gears have been reported [8–15] and their characteristics verified with experimental data. Reference [16] compared radial-flux, transverse-flux and

Received 3 March 2016, Accepted 26 April 2016, Scheduled 20 July 2016

* Corresponding author: Norhisam Misron (norhisam@upm.edu.my).

[1] Department of Electrical & Electronic, Faculty of Engineering, Universiti Putra Malaysia, 43400 UPM Serdang, Selangor, Malaysia.

[2] Institute of Advanced Technology, Faculty of Engineering, Universiti Putra Malaysia, 43400 UPM Serdang, Selangor, Malaysia.

[3] Department of Biological Functions Engineering, Graduate School of Life Science and Systems Engineering, Kyushu Institute of Technology, 2-4 Hibikino Wakamatsu-ku, Kitakyushu 808-0916, Japan.

axial flux-magnetic gears and concluded that radial-flux magnetic gears have superior torque density, but experimental data was not reported. The operating principle of a magnetic gear is similar to a mechanical gear where torque is transferred from a low speed shaft to a high speed shaft with permanent magnets. Studies [17–19] have shown that integrating a brushless permanent magnet machine with a magnetic gear could result in a compact and cost effective electromechanical machine.

The purpose of this paper is to propose a novel structure of double-stator permanent magnet generator integrated with a magnetic gear. The aim is to improve inefficient low speed and address problems with mechanical gears by integrating a magnetic gear designed with two modulating iron rings and three independent permanent magnet rotors. Electromechanical energy conversion is achieved by field excitation between two field permanent magnet rotors and two field windings in the stators. In Section 2, the proposed structure and basic operating principle of the machine will be discussed. Section 3 will present the finite element method. Section 4 discusses the results. Finally, the conclusion is presented in Section 5.

2. PROPOSED STRUCTURE AND OPERATING PRINCIPLE

2.1. Proposed Structure

Figure 1 shows the structure of the proposed machine. It comprises seven parts: the inner stator, the inner coil windings, the inner field PMs, the inner modulating iron ring, the prime PMs, the outer modulating iron ring, the outer field PMs, the outer stator and outer coil windings. The field PMs are mounted on both outer and inner rotors while the prime PMs are fixed on the middle rotor. A coaxial magnetic gear with three rotors is integrated with a double-stator generator to form a compact double-stator magnetic geared integrated generator.

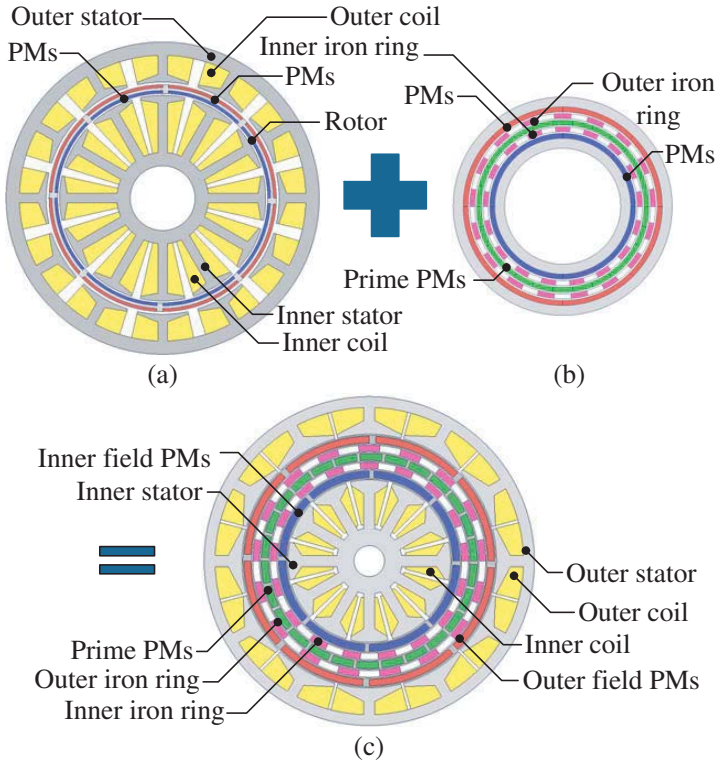

Figure 1. Integrated double-stator PM generator with magnetic gear. (a) DSPM generator. (b) Triple rotor MG. (c) DSPM generator integrated with MG.

2.2. Magnetic Gear Operating Principle

In this magnetic gear structure shown in Fig. 2, there is an outer rotor consisting of p_1 pole-pair field permanent magnets (PMs) rotating at ω_1; an outer iron ring consisting of n_2 ferromagnetic pole pieces with a rotational speed of ω_2; a middle rotor consisting of prime PMs rotating at ω_3; an inner iron ring comprising of n_4 ferromagnetic pole pieces with a rotational speed of ω_4; and an inner rotor consisting of p_5 pole-pair field PMs rotating at ω_5. The structure consists of an integrated outer and inner magnetic gear which operates with three independent PM rotors. If the relationship between the outer field PM poles and outer stationary ring pole pieces is chosen to be $p_1 = |p_3 - n_2|$ [20] and the inner field PM poles and inner stationary ring pole pieces is chosen to be $p_5 = |p_3 - n_4|$ the rotational angular speed relation between the two rotors in the outer gear is given as

$$\omega_1 = \frac{p_3}{p_3 - n_2}\omega_3 + \frac{n_2}{n_2 - p_3}\omega_2 \quad \text{[Outer magnetic gear]} \tag{1}$$

while the rotational angular speed relation between the two rotors in the inner gear is given as

$$\omega_5 = \frac{p_3}{p_3 - n_4}\omega_3 + \frac{n_4}{n_4 - p_3}\omega_4 \quad \text{[Inner magnetic gear]} \tag{2}$$

If both inner and outer field PMs rotate at the same velocity, applying the transitive law: $(\omega_{15} \to \omega_1) \wedge (\omega_1 \to \omega_5) \Longrightarrow \omega_{15} \to \omega_5$, i.e., $\omega_{15} = \omega_1 = \omega_5$, similarly if both inner and outer iron ring pole pieces are stationary $(\omega_{24} \to \omega_2) \wedge (\omega_2 \to \omega_4) \Longrightarrow \omega_{24} \to \omega_4$, i.e., $\omega_{24} = \omega_2 = \omega_4 = 0$ including equal number of inner and outer iron ring pole pieces $n_{24} = n_2 = n_4$ combining (1) and (2) the equation relating the three PM rotors can be reduced to

$$\omega_{15} = \frac{p_3}{p_3 - n_{24}}\omega_3 + \frac{n_{24}}{n_{24} - p_3}\omega_{24} \tag{3}$$

For the magnetic gear design $p_1 = p_5 = 4$ pole-pairs of outer and inner field PMs, $n_2 = n_4 = 17$ pole pieces of outer and inner iron ring and $p_3 = 13$ pole-pairs of prime PMs.

From Equation (3) this gives

$$\omega_{15} = 4.25\omega_{24} - 3.25\omega_3 \tag{4}$$

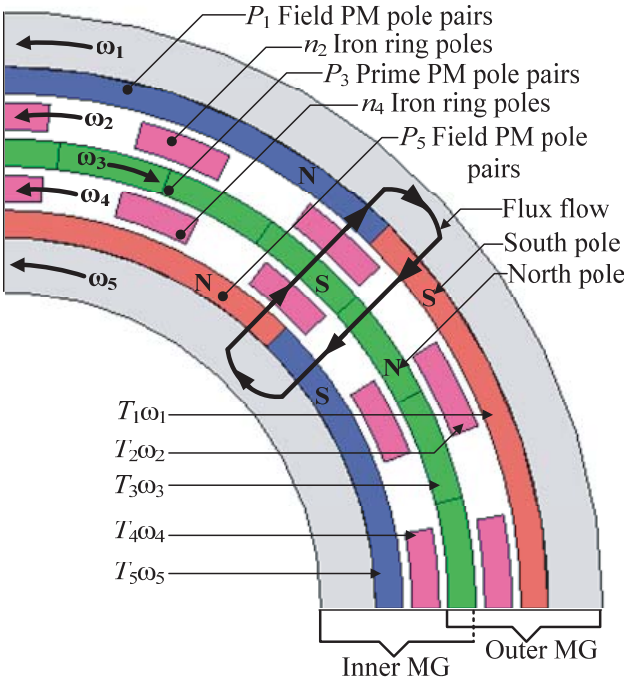

Figure 2. Triple rotor magnetic gear.

If both outer and inner PM rotors are stationary ($\omega_{15} = \omega_1 = \omega_5 = 0$) the gear ratio will be $1 : 4.25$. Similarly if both iron ring pole pieces are stationary ($\omega_{24} = \omega_2 = \omega_4 = 0$) the gear ratio will be $-1 : 3.25$.

If the iron ring pole pieces are static, i.e., $\omega_{24} = 0$ the gear ratio is given by

$$\omega_{15} = -\frac{p_3}{n_{24} - p_3}\omega_3 \tag{5}$$

If the prime PM rotor is static, i.e., $\omega_3 = 0$ the gear ratio is given as

$$\omega_{15} = \frac{n_{24}}{n_{24} - p_3}\omega_{24} \tag{6}$$

Applying the law of conservation of energy and neglecting power losses in the MG shown in Fig. 2, it yields

$$T_1\omega_1 + T_2\omega_2 + T_3\omega_3 + T_4\omega_4 + T_5\omega_5 = 0 \tag{7}$$

where T_1, T_2, T_3, T_4 and T_5 are the torques for the outer rotor, outer iron ring, prime rotor, inner iron ring and inner rotor, respectively. If the two iron rings are stationary ($\omega_2 = \omega_4 = 0$), it yields

$$T_1\omega_1 + T_3\omega_3 + T_5\omega_5 = 0 \tag{8}$$

If the outer and inner PM rotors rotate at the same speed due to the same gear ratio, i.e., $\omega_{15} = \omega_1 = \omega_5$ then substituting into (8) gives

$$T_1\omega_{15} + T_3\omega_3 + T_5\omega_{15} = 0 \tag{9}$$

$$T_3 = -\frac{\omega_{15}}{\omega_3}(T_1 + T_5) \tag{10}$$

$$G_r = \frac{\omega_{15}}{\omega_3} = -\frac{p_3}{n_{24} - p_3} \tag{11}$$

The equation which relates the magnetic torques on the three PM rotors for the magnetic gear is expressed as

$$G_r = -\frac{T_3}{T_1 + T_5} \tag{12}$$

The minus sign indicates that both outer and inner rotors rotate similarly but opposite in direction to the prime rotor. The pole-pair number p_1, p_3 ,p_5 and pole number of iron ring pieces $n_2 = n_4$ are selected as 4, 4, 13 and 17 respectively. This combination produces a gear ratio of $3.25 : 1$. The specifications of the proposed DSPMG integrated with MG are listed in Table 1 and the calculated rated speeds of the prime rotor, inner and outer rotors are 231 rpm and 750 rpm, respectively.

Table 1. Specifications of proposed DSPMG with MG.

Parameter	Value
Pole-pair number inner PMs	4
Pole-pair number outer PMs	4
Pole-pair number prime PMs	13
Pole number iron ring pieces	17
Outer and inner airgap [mm]	1
Inner rotor speed [rpm]	750
Outer rotor speed [rpm]	750
Prime rotor speed [rpm]	231
Power [kW]	1
Frequency [Hz]	50
Axial length [mm]	30
Outer diameter [mm]	151

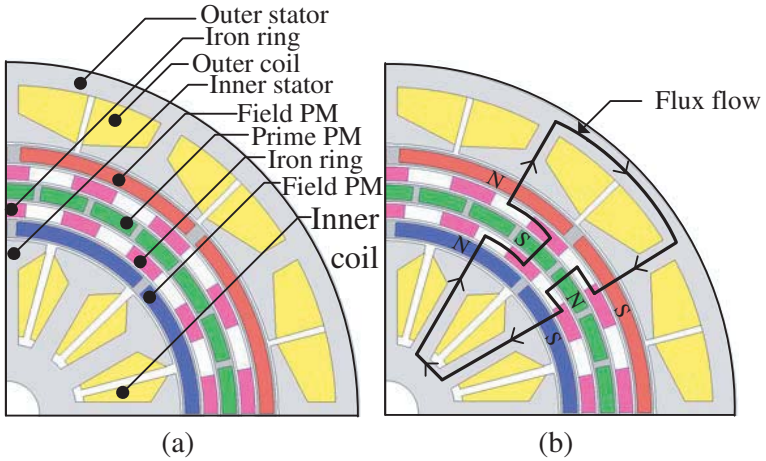

Figure 3. Structure of DSPMG integrated with magnetic gear. (a) 1/4 model of structure. (b) Flux flow.

2.3. Double-Stator Permanent Magnet Generator Operating Principle

The output electrical power of a DSPMG [21] produced from the voltage generated independently at the inner and outer stator is calculated as:

$$E_G = 4.44 f N \phi \quad [\text{V}] \tag{13}$$

where E_G is the generated rms voltage in Volts, f the frequency of the generator in Hertz, N the number of turns, and ϕ the magnetic flux through the coil winding in Weber. The quantity of current flowing through both inner and outer coils is calculated as:

$$I_a = \frac{E_G}{\sqrt{\left(R_a + R_L\right)^2 + \left(2\pi f L_c\right)^2}} \quad [\text{A}] \tag{14}$$

where I_a is the current, R_a the armature resistance of the coil winding, R_L the load resistance, and L_c the coil inductance. The total machine loss of a DSPMG is given by:

$$P_l = I_a^2 R_C + \varepsilon_h f B^\alpha + \varepsilon_e f^2 B^2 \quad [\text{W}] \tag{15}$$

where P_l is the total losses power, ε_h the hysteresis coefficient, ε_e the eddy current coefficient, α a constant, and B the flux density of the magnet. The total output power P_{out} generated is calculated based on Equation (16).

$$P_{\text{out}} = \left(E_G - E_a\right) I_a - P_l \quad [\text{W}] \tag{16}$$

The total output power P_t combined for both inner and outer stators in a DSPM generator is

$$P_t = \left[\left(E_{G\_\text{out}} - E_{a\_\text{out}}\right) I_{a\_\text{out}} - P_{l\_\text{out}}\right] + \left[\left(E_{G\_\text{in}} - E_{a\_\text{in}}\right) I_{a\_\text{in}} - P_{l\_\text{in}}\right] \quad [\text{W}] \tag{17}$$

3. FINITE ELEMENT METHOD

A two-dimension finite element method (2D-FEM) numerical tool is used to evaluate the performance characteristics of the proposed machine. The two-dimensional electromagnetic equation governed by Maxwell's equation is given as:

$$\Omega : \frac{\partial}{\partial x}\left(\gamma \frac{\partial y}{\partial x}\right) + \frac{\partial}{\partial y}\left(\gamma \frac{\partial y}{\partial y}\right) = -J - \gamma\left(\frac{\partial B_{ry}}{\partial x} - \frac{\partial B_{rx}}{\partial y}\right) + \sigma \frac{\partial A}{\partial t} \tag{18}$$

where Ω is the field solution region of calculation, A the magnetic vector potential, J the current density, σ the electrical conductivity, and B_{rx} and B_{ry} are the remanent flux density. The back-electromagnetive force (Back-EMF) of the coil winding can be expressed as:

$$e = -\frac{L}{S}\left(\iint_{\Omega+} \frac{\partial A}{\partial t} d\Omega - \iint_{\Omega-} \frac{\partial A}{\partial t} d\Omega\right) \tag{19}$$

where e is the Back-EMF generated by one coil, L the axial length of the machine, S the area of conductor of each phase winding, and $\Omega+$ and $\Omega-$ are the cross sectional areas of the input and output conductor coil [22].

4. RESULTS AND DISCUSSION

4.1. Flux Density Distribution and Harmonic Analysis

In Fig. 4(a), there is minimum leakage of magnetic flux at the outer stator since the stator pole shoe is wider, and the flux flows across the airgap with less fringing flux. Also both inner and outer field permanent magnets have a pole-arc pitch angle of 42°. This results to decrease in the permeance of the magnets and electromagnetic torque but in real practice the full magnet pole-arc is rarely used because of manufacturing considerations and effect on the cogging torque. In Fig. 4(b) it is observed that the magnetic flux density is concentrated more at the outer stator back iron and inner stator pole core because the magnetic flux flows through the shortest path.

Figures 6(a), (c), (e) show the radial component of the magnetic flux density waveform in the middle of the three inner air gaps due to the inner field PMs and prime PMs while Figs. 6(b), (d), (f) show their harmonic order. The number of flux density pulsations within a period is governed by the number of PMs and stationary pole-pieces. The period of magnetic flux density within the inner

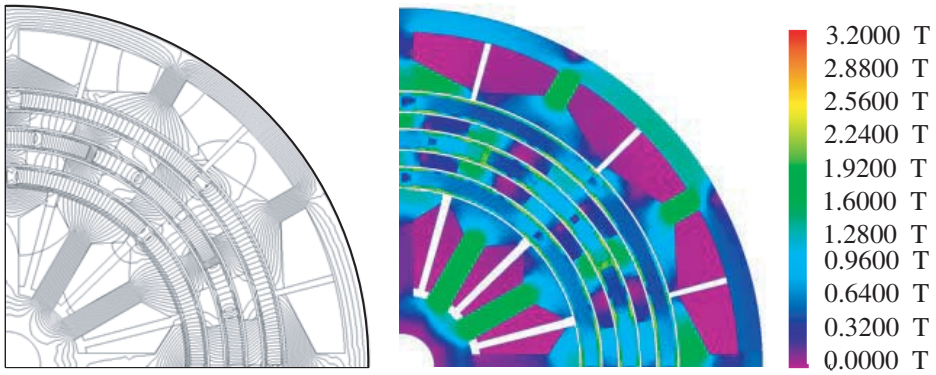

Figure 4. Magnetic field and flux distribution. (a) Magnetic field distribution. (b) Magnetic flux distribution.

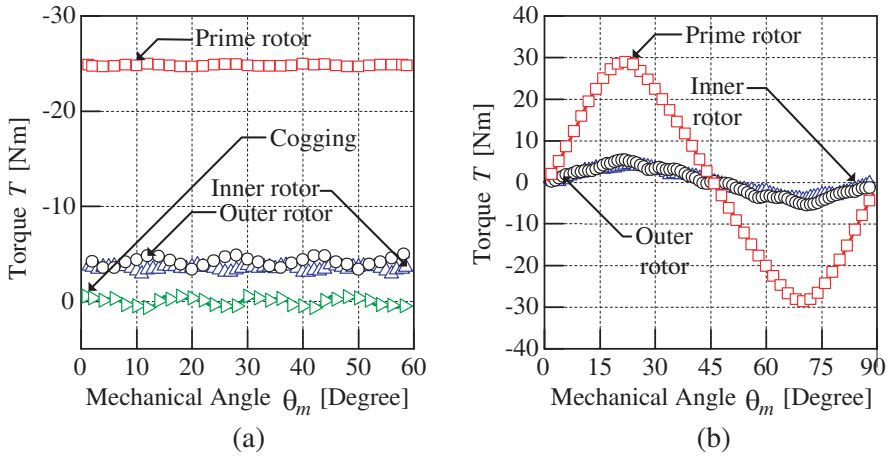

Figure 5. Torque waveform characteristics. (a) Transmission and cogging torque. (b) Pull-out torque angle curves.

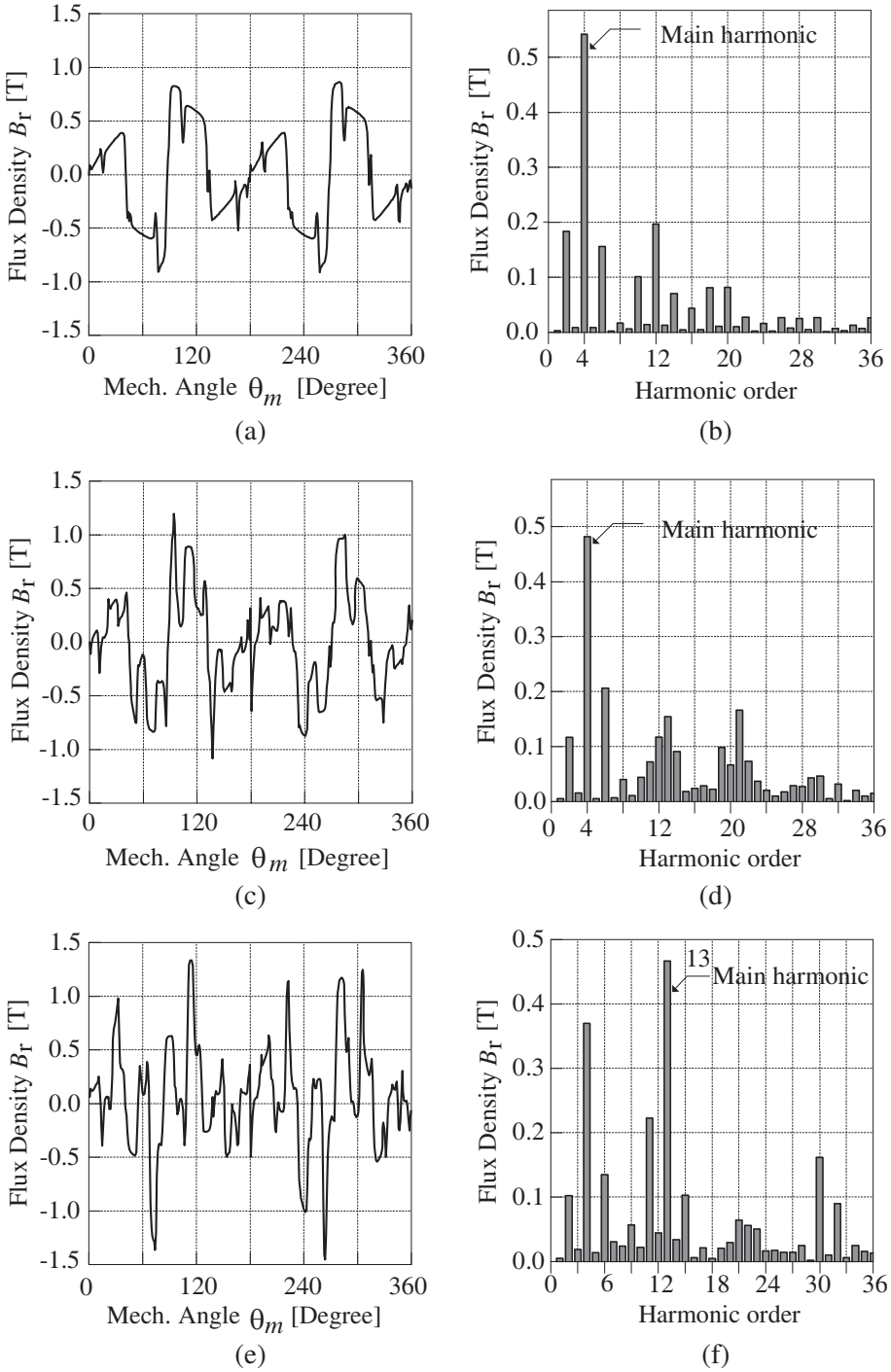

Figure 6. The magnetic flux density waveforms in three inner air-gaps. (a) Between inner stator and PM. (b) FFT from (a). (c) Between PM and iron ring. (d) FFT from (c). (e) Between iron ring and PM. (f) FFT from (e).

air gap between the inner field PMs and stationary pole-pieces is $360°/4 = 90°$. The number of flux density pulsations is equal to the number of field PMs (8 poles) on the inner rotor. Also the effect of flux concentration results to dominant magnetic flux pulsation within the inner air gap at 90°, and 280°. It can be observed that the stationary ring pole pieces modulates the magnetic fields produced by

the PMs resulting to a number of asynchronous space harmonics, viz $k \neq 1$. The asynchronous space harmonic having the largest amplitude with order of 4th space harmonic, ($m = 1$, $k = -1$) pairs with the 4 pole-pair high speed PMs to transmit electromagnetic torque at a rotational speed of:

$$\omega_o = -3.25\omega_i \tag{20}$$

Figures 7(a), (c), (e) show the radial component of the magnetic flux density waveform in the middle

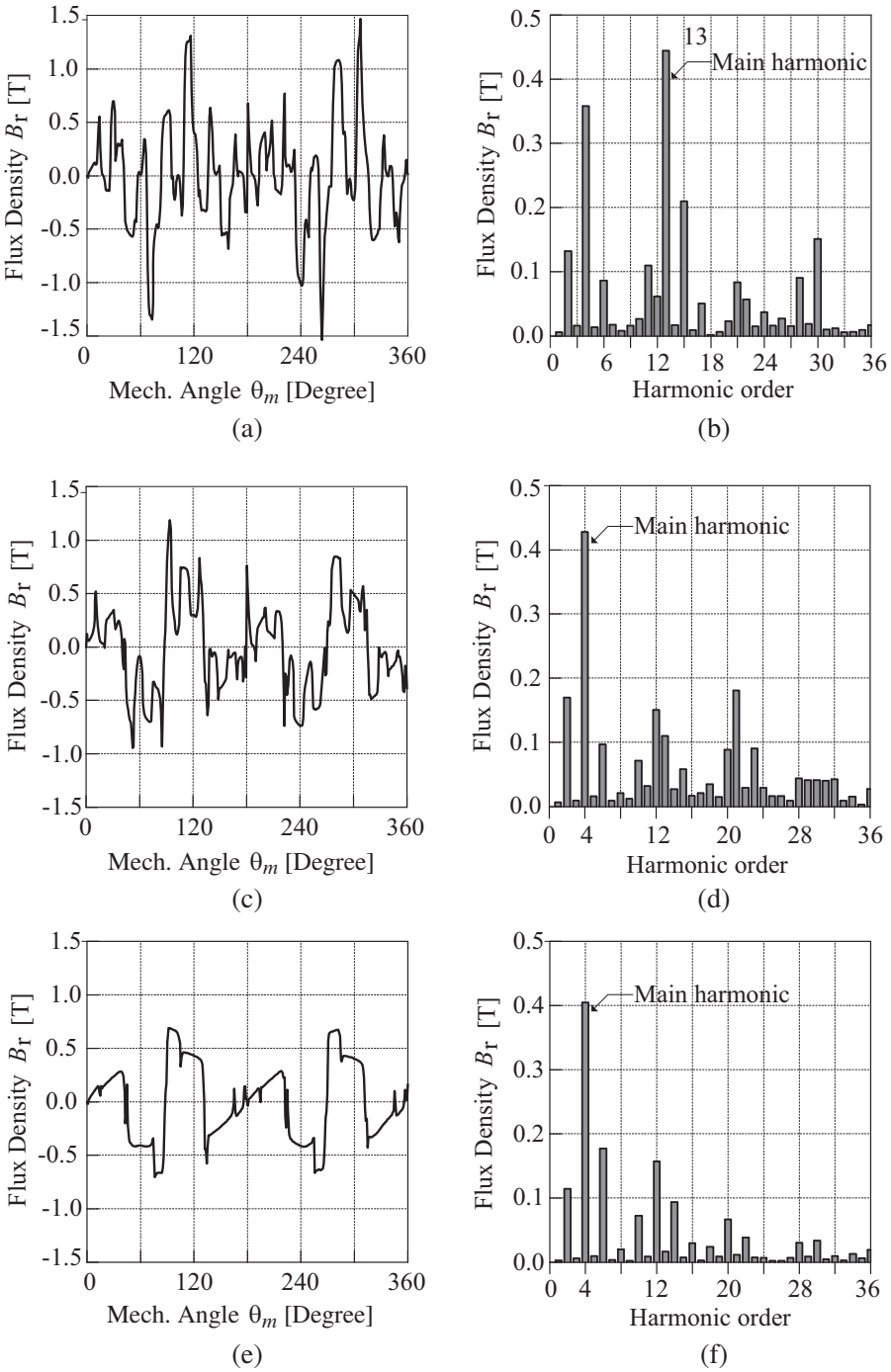

Figure 7. The magnetic flux density waveforms in three outer air-gaps. (a) Between prime PM and iron ring. (b) FFT from (a). (c) Between iron ring and PM. (d) FFT from (c). (e) Between PM and outer stator. (f) FFT from (e).

of the outer air gaps due to the prime PMs and outer field PMs while Figs. 7(b), (d), (f) show their harmonic order. The number of flux density pulsations within a period is governed by the number of PMs and stationary pole-pieces. The period of magnetic flux density within the outer air gap between the prime PMs and stationary pole-pieces is $360°/13 = 27.69°$. The number of flux density pulsations is equal to the number of prime PMs (26 Poles) on the middle rotor. Also the effect of flux concentration results to dominant magnetic flux pulsation within the inner and outer air gaps at 115°, 280° and 305°. By applying Fast Fourier Transform (FFT), it can be seen that the presence of the stationary ring pole-pieces results to a number of asynchronous space harmonics, viz $k \neq 1$, the largest amplitude 13th space harmonic order ($m = 1$, $k = -1$), pairs with the 13 pole-pair low speed PMs to transmit electromagnetic torque at a gear ratio of:

$$\frac{\omega_o}{\omega_i} = \frac{P_o}{P_i - n_s} = -3.25 : 1 \tag{21}$$

4.2. Transmission and Cogging Torque Characteristics

Figure 5(a) illustrates the average transmission torques of the three PM rotors in the magnetic gear and their simulation results are 24.80 Nm, 3.47 Nm and 4.16 Nm respectively. The simulated transmission torque ratio is 1 : 3.25, which is equal to the calculated ratio of pole-pair numbers for the three rotors. The maximum torque-angle curves of the three PM rotors shown in Fig. 5(b) are calculated by holding the prime rotor static while both inner and outer rotors are rotated step by step. It can be observed that the torque-angle curve is sinusoidal and the maximum torque value indicates the pull-out torques. The pull-out torques on the inner rotor, outer rotor and prime rotors are 3.90 Nm, 4.91 Nm and 28.58 Nm respectively. The ratio of the pull-out torques for the three PM rotors is 1 : 3.24, which is 99.7% accurate with the calculated magnetic gear ratio of 1 : 3.25. The torque ripple results from the interaction of both outer and inner PMs with the iron ring pole-pieces because there is variation in the reluctance between the iron rings and permanent magnets. Fig. 5(a) shows that the torque ripple on both outer and inner rotors is more prominent than on the prime rotor.

4.3. Electrical Power Characteristics

If the generator is operating at rated speeds ($\omega_1 = 231$ rpm, $\omega_2 = 750$ rpm) the back-EMF waveform is shown in Fig. 8(a) while the harmonic spectrum is calculated with Fast Fourier Transform (FFT) and is illustrated in Fig. 8(b). The amplitude of the fundamental frequency when the generator is coupled to a resistive load of 3 Ω per phase is 29.18 V and the fundamental component frequency = 50 Hz. Fig. 9(a) shows the electric power generated on a resistive load of 5 Ω after full rectification. The power curve

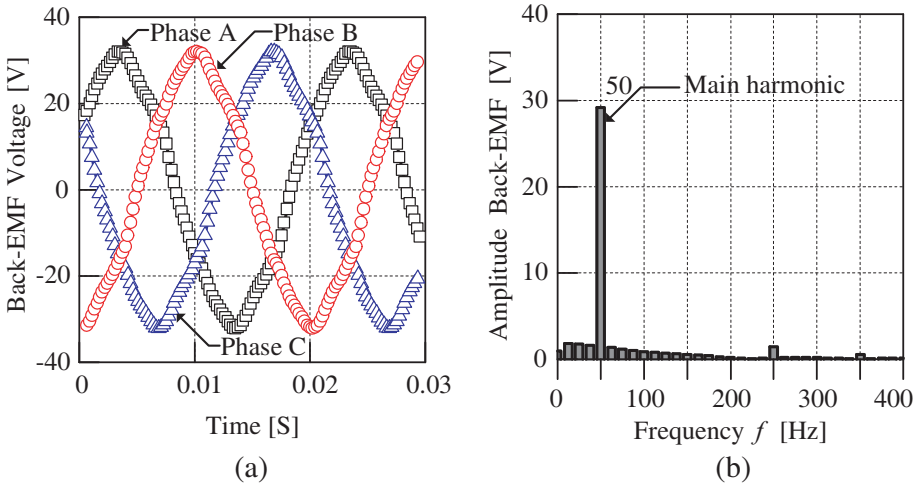

Figure 8. Phase back-EMF at rated speed. (a) Back-EMF voltage. (b) Harmonic spectra.

is linear from 650 rpm to 2500 rpm, while at 4000 rpm the curve dips and it can be observed that at 7000 rpm the electric power is at saturation point. The DC voltage generated after full rectification is illustrated in Fig. 9(b) and it shows that at 5000 rpm the DC voltage generated does not increase beyond 108 V which shows the machine has reached saturation point. This observation is also consistent with Fig. 9(c) in which the load current I is maximum at 21 A from 6000 rpm.

In Fig. 9(a) when the resistance load is 5 ohm, the power curve shows saturation above 1200 W. This observation is similar for the voltage and current shown in Fig. 9(b) and Fig. 9(c), respectively. The power efficiency map illustrated in Fig. 10(a) shows that when the resistance load is constant with varied speed, the power increases until a peak point of saturation is reached. At a resistance load of 15 ohm maximum power is transferred and when the load resistance is increased, the power reduces since the external load is approximately equal to the generator's internal resistance. This shows that by varying the load resistance on the generator, maximum power is achieved by impedance matching of both load and generator resistances. The predicted efficiency of the generator is calculated at various load resistances and operating speeds. Fig. 10(b) shows the predicted efficiency graph curve. It can be observed that the efficiency increases proportionally with load resistance up to saturation point after which further increase results to decrease in efficiency as a result of losses. The calculated efficiency of

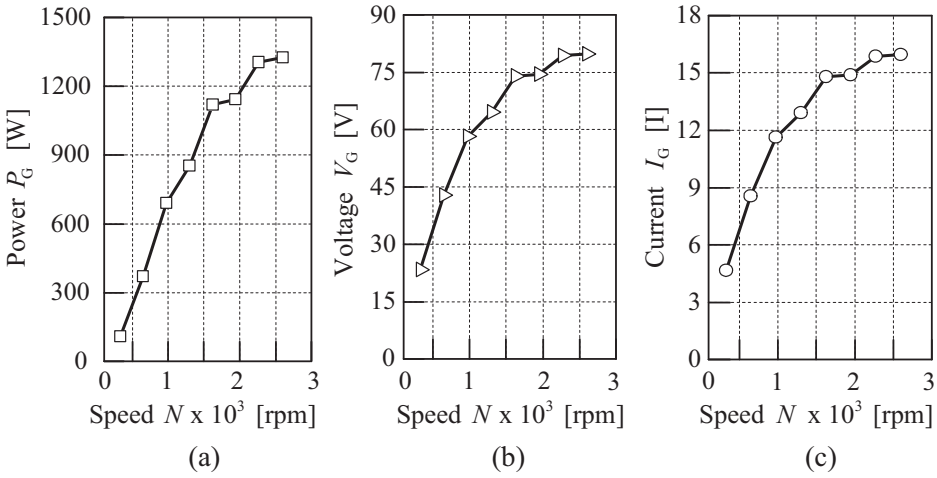

Figure 9. Generator power characteristics. (a) Power/speed curve. (b) Voltage/speed curve. (c) Current/speed curve.

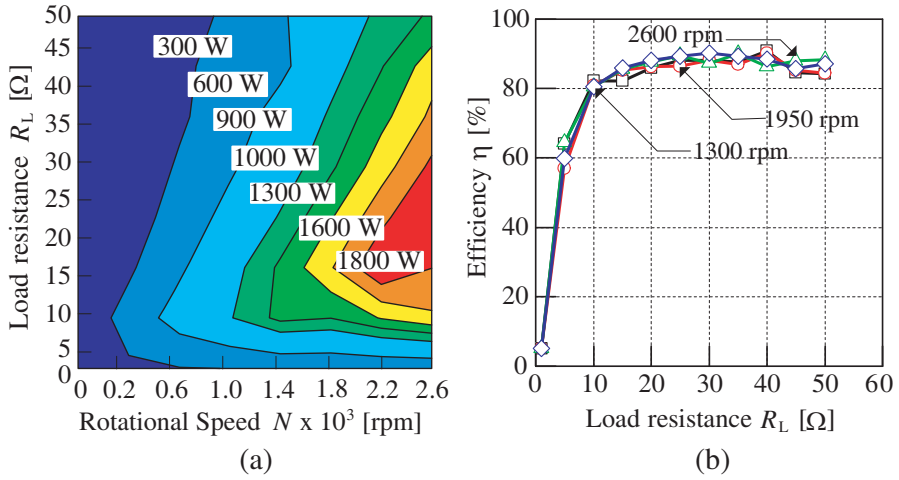

Figure 10. Power mapping and efficiency of generator. (a) Generator power mapping. (b) Efficiency curve.

the generator is 88% on-load with copper and iron losses. The machine's operating efficiency varies with speed and load. It can be observed in Fig. 10(b) that at variable speed the efficiency curve converges between 85%–90% for various load resistance.

If the generator is to operate based on the proposed design, the magnetic gear's transmission torque should be greater than the torque produced by the generator for it to rotate smoothly, or it will stall. In Table 2, it is observed that the transmission torque of both inner and outer rotors is greater than the generator's torque produced at both inner and outer stators, respectively. The torque produced by the prime rotor on no-load is calculated as 24.80 Nm, but the simulation results show a torque of 22.14 Nm on load at 89.27% efficiency. This decrease in torque is as a result of copper and iron losses but not much to affect the performance of the generator. It is observed that the total torque produced by both inner and outer rotors is greater than the total torque generated at the inner and outer stators by a factor of 2. This validates the operating principle of the proposed generator design.

Table 2. Performance characteristics at ($N_{\text{field}} = 1950\,\text{rpm}$, $N_{\text{prime}} = 600\,\text{rpm}$, $R_L = 15\,\Omega$).

Generator		Magnetic Gear	
Output power [W]	1383.22	Pole pairs: p_1, $n_2 = n_4, p_3$	4, 17, 13
Iron losses [W]	34.95	Gear ratio	3.25
Copper losses [W]	159.14	Cogging, T_{cog} [Nm]	0.60
Efficiency [%]	85.97	Prime rotor, T_{prime} [Nm]	22.14
$\text{Stator}_{\text{outer}}$, T_{is} [Nm]	3.34	Outer rotor, T_{outer} [Nm]	7.24
$\text{Stator}_{\text{inner}}$, T_{os}[Nm]	3.40	Inner rotor, T_{inner} [Nm]	6.44
$T_{\text{total}} = T_{\text{is}} + T_{\text{os}}$ [Nm]	6.74	$T_{\text{total}} = T_{\text{inner}} + T_{\text{outer}}$ [Nm]	13.68

5. CONCLUSION

In this paper, a novel structure of double-stator permanent magnet generator integrated with a magnetic gear has been proposed, and its performance characteristics have been analyzed with 2-D FEM. The performance characteristics show that when the machine functions as a magnetic gear, the ratio of the transmission torque between the prime PMs and field PMs is 1 : 3.25, and the gear can scale up the rotational speed of both outer and inner rotor field PMs. It was found that for various load resistances at variable speeds, the calculated efficiency of the generator was 88%. Also the FEM analysis showed that the transmission torque of the magnetic gear was greater than the torque produced by the generator on load with generated power of 1 kW, therefore validating the proposed machine design. The proposed machine can be applied in wind power turbines to address inefficient power generation in low wind speed conditions by directly coupling the prime rotor to the wind turbine blades. The proposed generator has a complex mechanical structure, but future research can lower manufacturing cost by better utilization of PMs and ferromagnetic materials using optimization. Future work related to this study will construct a prototype for experimental validation.

REFERENCES

1. Li, X., K.-T. Chau, M. Cheng, and W. Hua, "Comparison of magnetic-geared permanent magnet machines," *Progress In Electromagnetics Research*, Vol. 133, 177–198, 2013
2. Rens, J., K. Atallah, S. Calverley, and D. Howe, "A novel magnetic harmonic gear," *IEEE Transactions on Industry Applications*, Vol. 46, No. 1, 206–212, 2010.
3. Jian, L. and K. Chau, "A coaxial magnetic gear with halbach permanent-magnet arrays," *IEEE Transactions on Energy Conversion*, Vol. 25, No. 2, 319–328, 2010.
4. Zhang, X., X. Liu, C. Wang, and Z. Chen, "Analysis and design optimization of a coaxial surface-mounted permanent-magnet magnetic gear," *Energies*, Vol. 7, No. 12, 8535–8553, 2014.

5. Atallah, K., J. Wang, S. Mezani, and D. Howe, "A novel high-performance linear magnetic gear," *IEEJ Trans. IA*, Vol. 126, No. 10, 1352–1356, 2006.
6. Mezani, S., K. Atallah, and D. Howe, "A high-performance axial-field magnetic gear," *J. Appl. Phys.*, Vol. 99, No. 8, 08R303, 2006.
7. Acharya, V., J. Bird, and M. Calvin, "A flux focusing axial magnetic gear," *IEEE Trans. Magn.*, Vol. 49, No. 7, 4092–4095, 2013.
8. Jorgensen, F., T. Andersen, and P. Rasmussen, "The cycloid permanent magnetic gear," *IEEE Transactions on Industry Applications*, Vol. 44, No. 6, 1659–1665, 2008.
9. Niguchi, N. and K. Hirata, "Transmission torque analysis of a novel magnetic planetary gear employing 3-D FEM," *IEEE Trans. Magn.*, Vol. 48, No. 2, 1043–1046, 2012.
10. Niguchi, N. and K. Hirata, "Cogging torque analysis of magnetic gear," *IEEE Trans. Ind. Electron.*, Vol. 59, No. 5, 2189–2197, 2012.
11. Tsai, M. and L. Ku, "3-D printing-based design of axial flux magnetic gear for high torque density," *IEEE Trans. Magn.*, Vol. 51, No. 11, 1–4, 2015.
12. Uppalapati, K., W. Bomela, J. Bird, M. Calvin, and J. Wright, "Experimental evaluation of low-speed flux-focusing magnetic gearboxes," *IEEE Transactions on Industry Applications*, Vol. 50, No. 6, 3637–3643, 2014.
13. Holm, R., N. Berg, M. Walkusch, P. Rasmussen, and R. Hansen, "Design of a magnetic lead screw for wave energy conversion," *IEEE Transactions on Industry Applications*, Vol. 49, No. 6, 2699–2708, 2013.
14. Jing, L., L. Liu, M. Xiong, and D. Feng, "Parameters analysis and optimization design for a concentric magnetic gear based on sinusoidal magnetizations," *IEEE Trans. Appl. Supercond.*, Vol. 24, No. 5, 1–5, 2014.
15. Huang, C.-C., M.-C. Tsai, D. Dorrell, and B.-J. Lin, "Development of a magnetic planetary gearbox," *IEEE Trans. Magn.*, Vol. 44, No. 3, 403–412, 2008.
16. Chen, Y., W. Fu, S. Ho, and H. Liu, "A quantitative comparison analysis of radial-flux, transverse-flux, and axial-flux magnetic gears," *IEEE Trans. Magn.*, Vol. 50, No. 11, 1–4, 2014.
17. Frandsen, T., L. Mathe, N. Berg, R. Holm, T. Matzen, P. Rasmussen, and K. Jensen, "Motor integrated permanent magnet gear in a battery electrical vehicle," *IEEE Transactions on Industry Applications*, Vol. 51, No. 2, 1516–1525, 2015.
18. Liu, C.-T., H.-Y. Chung, and C.-C. Hwang, "Design assessments of a magnetic-geared double-rotor permanent magnet generator," *IEEE Transactions on Magnetics*, Vol. 50, No. 1, 1–4, 2014.
19. Liu, C., K. T. Chau, and Z. Zhang, "Novel design of double-stator single-rotor magnetic-geared machines," *IEEE Transactions on Magnetics*, Vol. 48, No. 11, 4180–4183, 2012.
20. Atallah, K., S. D. Calverley, and D. Howe, "Design, analysis and realisation of a high performance magnetic gear," *IEE Proc. — Electr. Power Appl.*, Vol. 151, 135–143, Mar. 2004.
21. Norhisam, M., S. Ridzuan, R. Firdaus, C. Aravind, H. Wakiwaka, and M. Nirei, "Comparative evaluation on power-speed density of portable permanent magnet generators for agricultural application," *Progress In Electromagnetics Research*, Vol. 129, 345–363, 2012.
22. Jian, L., K. Chau, and J. Jiang, "A magnetic-geared outer-rotor permanent-magnet brushless machine for wind power generation," *IEEE Transactions on Industry Applications*, Vol. 45, No. 3, 954–962, 2009.